INTERNATIONAL JOURNAL FOR NUMERICAL AND ANALYTICAL METHODS IN GEOMECHANICS, VOL. 20, 489–516 (1996)

UNDRAINED CAVITY EXPANSIONS IN CRITICAL STATE SOILS

I. F. COLLINS*

Department of Engineering Science, The University of Auckland, Private Bag 92019, New Zealand

H. S. YU†

Department of Civil Engineering and Surveying, The University of Newcastle, N.S.W. 2308, Australia

SUMMARY

Boundary value problems for hardening/softening soils, such as Cam-Clay, usually require the extensive use of finite element methods. Here analytical and semi-analytical solutions for the undrained expansion of cylindrical and spherical cavities in critical state soils are presented. The strain is finite, the initial cavity radius is arbitrary and the procedure applicable to any isotropically hardening materials. In all cases only simple quadratures are involved, and in the case of the original Cam-Clay a complete analytical solution can be found. In addition to providing models of the behaviour of displacement piles and pressuremeters these results also provide valuable benchmark solutions for verifying various numerical methods.

KEY WORDS: cavity expansion; critical state models; plasticity; pile installation; normally and overconsolidated clays

INTRODUCTION

Over the last 30 years, cavity expansion theory has been used widely in geotechnical engineering to model *in situ* soil testing (e.g. pressuremeters and cone penetrometers), pile driving and tunnelling. Until fairly recently the analysis of cavity expansion problems has mainly been based upon *elastic–perfectly plastic* soil models.[1–11] Some of these references include the effects of dilatancy by employing non-associated flow rules. Carter and co-workers[12,13] have used finite element methods to study the expansion of cavities in materials exhibiting hardening/softening such as Cam-Clay. More recently, Collins *et al.*[14,15] have produced semi-analytical solutions for cavities expanding under drained conditions from zero initial radius (i.e. created cavities) in sands using the state parameter model of Been and Jefferies.[16] The solutions were found by using similarity solutions techniques. Essentially, the same procedure has been used by Collins and Stimpson[17] to solve the drained and undrained, created cavity expansion problems for clays. The similarity solutions corresponding to cavities with zero initial radius can be viewed as *intermediate asymmptotic* solutions which are approached by the solution of a finite sized initial cavity, at large strains, when the cavity has 'forgotten' its initial size. These similarity solutions provide predictions of the limit effective and excess pore pressures. Instead of using plasticity theory, Davis *et al.*[18] showed that a rate-type (or hypoelastic) stress–strain relationship can also be used to obtain some useful solutions for undrained expansion of a created cylindrical cavity in clays. Solutions for cavities expanding from a finite initial radius in sand (as in a self-boring pressuremeter test) with a state parameter constitutive model have been obtained most recently by Yu[19,20] using finite elements.

† Senior Lecturer, Corresponding author
* Professor

CCC 0363–9061/96/070489–28

Received 12 May 1995
Revised 24 October 1995

The present paper is concerned with undrained cavity expansions in both normally and overconsolidated clays. The soil is modelled by a variety of Cam-Clay critical state models.[21-23] The assumption of zero initial radius is relaxed since the volume constancy of an undrained expansion introduces other simplifications into the analysis. It is hence now possible to produce solutions for cylindrical cavities which model the action of the pressuremeter, and for spherical cavities that may be used to estimate cone tip resistance and bearing capacity of displacement piles. It is further possible to ascertain how quickly the finite cavity solution settles down to the similarity solution. In undrained deformations it is common to work with total stresses. However, this is no longer appropriate in models in which the strength of the soil is a variable, since the strength is a function of the effective stresses rather than the total stresses. In particular, unlike the effective stress approach, the total stress analysis cannot take acount of the influence of soil stress history on the behaviour of the soil. Four fundamental equations occur in analysing cavity expansions: (a) conservation of mass or 'continuity', (b) quasi-static equilibrium, (c) the yield condition and (d) the elastic/plastic flow rule. In an undrained expansion (a) is automatically satisfied since the total volume of each soil element remains constant. This results in a simple relation between the finite shear strain and the position co-ordinates of the element, which is valid in both the elastic and plastic regions. The equilibrium condition (b) serves only to determine the excess pore pressure distribution at the end of the calculation after the effective stress distributions have been found by integrating the constitutive equations (c) and (d). Since for isotropic materials these two equations are most naturally expressed in terms of the effective mean and deviatoric stresses, the distributions of the effective stress components are most conveniently found by first solving for these two stress invariants.

KINEMATICS OF CAVITY EXPANSIONS

Since an undrained deformation is necessarily isochoric, the conservation of volume condition gives the following relation between r, the current radius of a material element which was initially at r_0 and the current and initial radii of the cavity–a and a_0, respectively (Figure 1):

$$r^{k+1} - r_0^{k+1} = a^{k+1} - a_0^{k+1} \tag{1}$$

where k is an index parameter used to denote cylindrical ($k = 1$) and spherical cavities ($k = 2$). The radial speed of the element is hence related to the speed of expansion of the cavity by

$$w = \dot{r} = \left(\frac{a}{r}\right)^k \dot{a} \tag{2}$$

So that the radial, circumferential, shear and volumetric strain rates can be expressed as follows:

$$e_r = -\frac{\partial w}{\partial r} = \left[\frac{ka^k}{r^{k+1}}\right]\dot{a} \tag{3}$$

$$e_\theta = -\frac{w}{r} = -\left[\frac{a^k}{r^{k+1}}\right]\dot{a} \tag{4}$$

$$\dot{\gamma} = e_r - e_\theta = \left[(k+1)\frac{a^k}{r^{k+1}}\right]\dot{a} \tag{5}$$

$$\dot{\delta} = e_r + ke_\theta = 0 \tag{6}$$

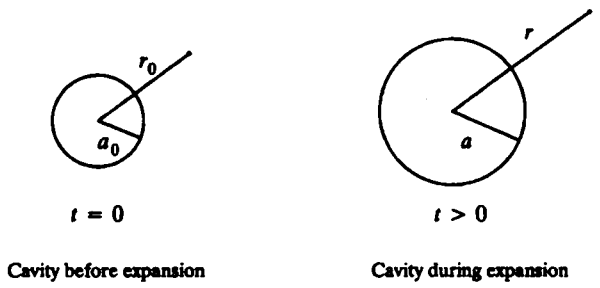

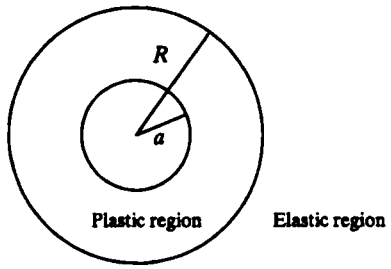

Cavity expansion at a particular instant

Figure 1. Kinematics of cavity expansion

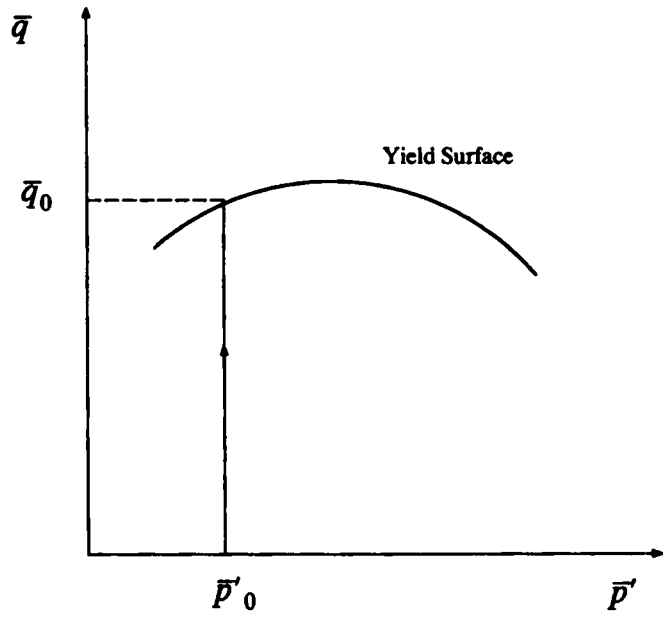

Figure 2. Stress path for elastic phase of cavity expansion

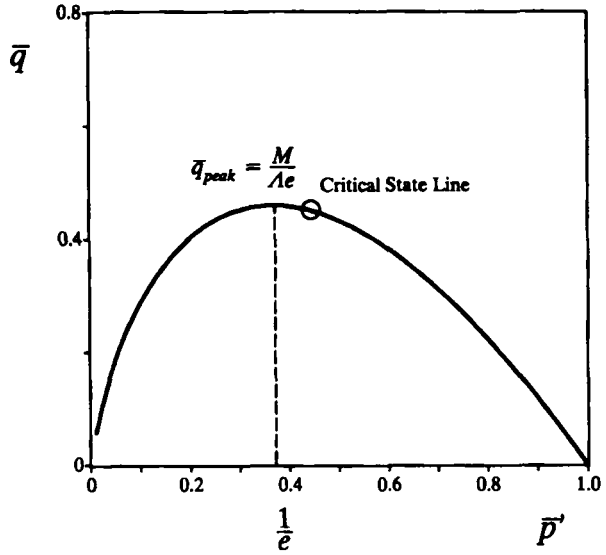

Figure 3. The original Cam-Clay yield surface

Using equation (1) the shear strain rate can also be written in terms of the initial position of the particle r_0:

$$\dot{\gamma} = \left[\frac{(k+1)a^k}{(a^{k+1} + r_0^{k+1} - a_0^{k+1}}\right]\dot{a} \tag{7}$$

Since r_0 is fixed for a given particle, (7) can be integrated to give the finite Lagrangean shear strain:

$$\gamma = \ln\left(\frac{a^{k+1} + r_0^{k+1} - a_0^{k+1}}{r_0^{k+1}}\right) = (k+1)\ln\frac{r}{r_0} \tag{8}$$

associated with the particle originally at r_0. This relation can now be written back in terms of r, the current co-ordinate of the particle:

$$\gamma = -\ln\left[1 - \frac{(a^{k+1} - a_0^{k+1})}{r^{k+1}}\right] \tag{9}$$

or inversely:

$$r^{k+1} = \frac{a^{k+1} - a_0^{k+1}}{1 - \exp(-\gamma)} \tag{10}$$

by using (1) to eliminate r_0. This expression gives the distribution of shear strain with radius r at the instant when the current cavity radius is a. From (8)–(10), it follows that the relations between radial and shear strain increments (a) for a given particle and (b) at a fixed instant of time are, respectively,

$$(k+1)\frac{dr}{r} = d\gamma \quad \text{and} \quad (k+1)\frac{dr}{r} = -\frac{d\gamma}{\exp(\gamma) - 1} \tag{11}$$

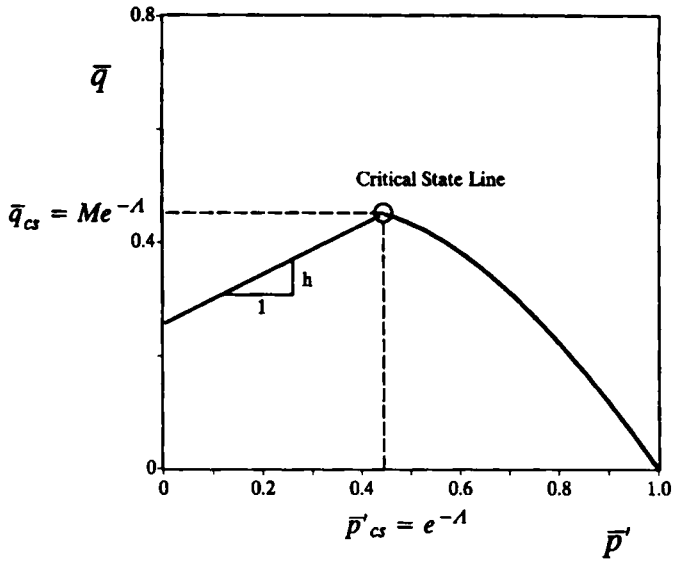

Figure 4. The original Cam-Clay–Hvorslev yield surface

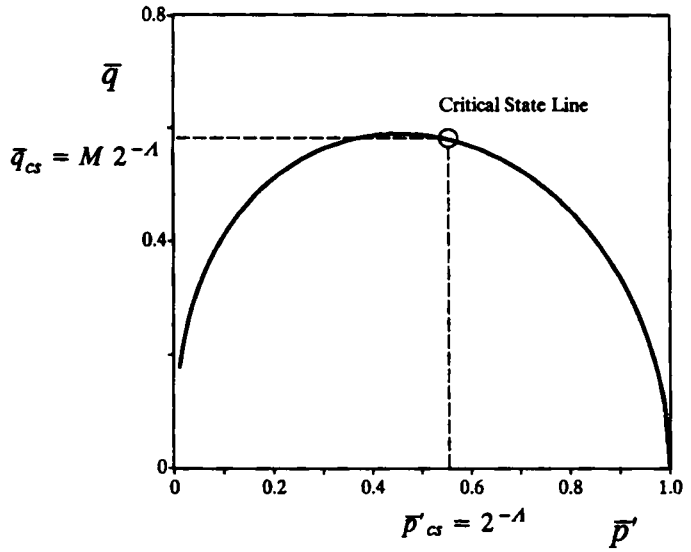

Figure 5. The modified Cam-Clay yield surface

Note that at the cavity wall the shear strain is

$$\gamma_c = (k+1)\ln\frac{a}{a_0} \tag{12}$$

which is infinite when the initial cavity radius is zero. It is to be emphasized that these results are kinematic and apply in both the elastic and elastic/plastic phases of the expansion.

ELASTIC PHASE OF EXPANSIONS

Following Collins and Stimpson,[17] the two effective stress invariants defined below are used for analysing cavity expansion problems:

$$q = \sigma'_r - \sigma'_\theta \quad \text{and} \quad p' = \frac{\sigma'_r + k\sigma'_\theta}{1 + k} \tag{13}$$

where σ'_r and σ'_θ are the effective radial and hoop stresses, respectively. In order to fuly take account of the scaling laws it is convenient to non-dimensionalise all stresses and moduli by some representative stress. Such non-dimensional variables will be denoted by superposed bars. Here we adopt the usual convention in critical state soil mechanics and use the equivalent consolidation pressure p'_e as this representative pressure. The elastic constitutive law is most conveniently expressed in rate form:

$$\dot{\delta}^e = \frac{\dot{\bar{p}}'}{\bar{K}(\bar{p}', v)} \quad \text{and} \quad \dot{\gamma}^e = \frac{\dot{\bar{q}}}{2\bar{G}(\bar{p}, v)} \tag{14}$$

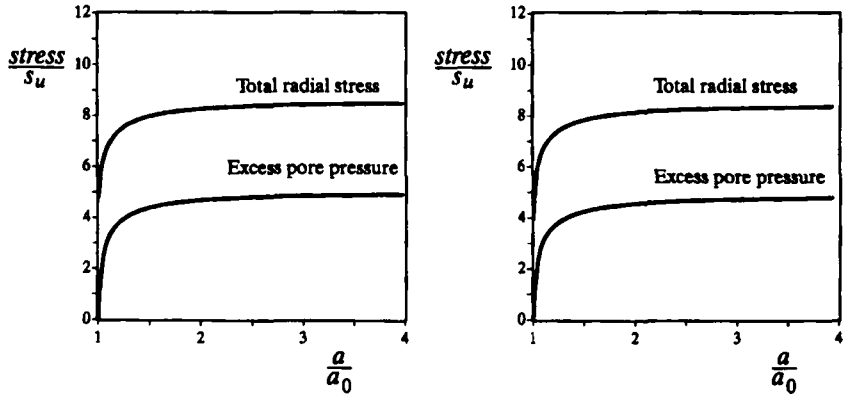

(a) Cylindrical Cavity in Original Cam-Clay

(b) Cylindrical Cavity in Modified Cam-Clay

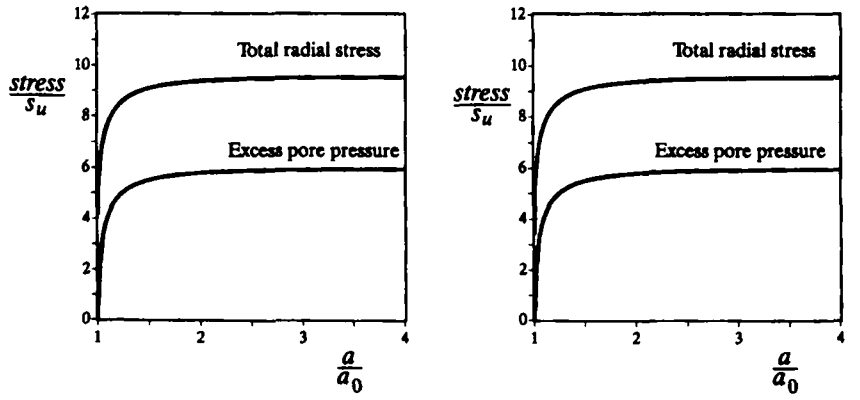

(c) Spherical Cavity in Original Cam-Clay

(d) Spherical Cavity in Modified Cam-Clay

Figure 6. Cavity expansion curves for OCR of $n_p = 1{\cdot}001$

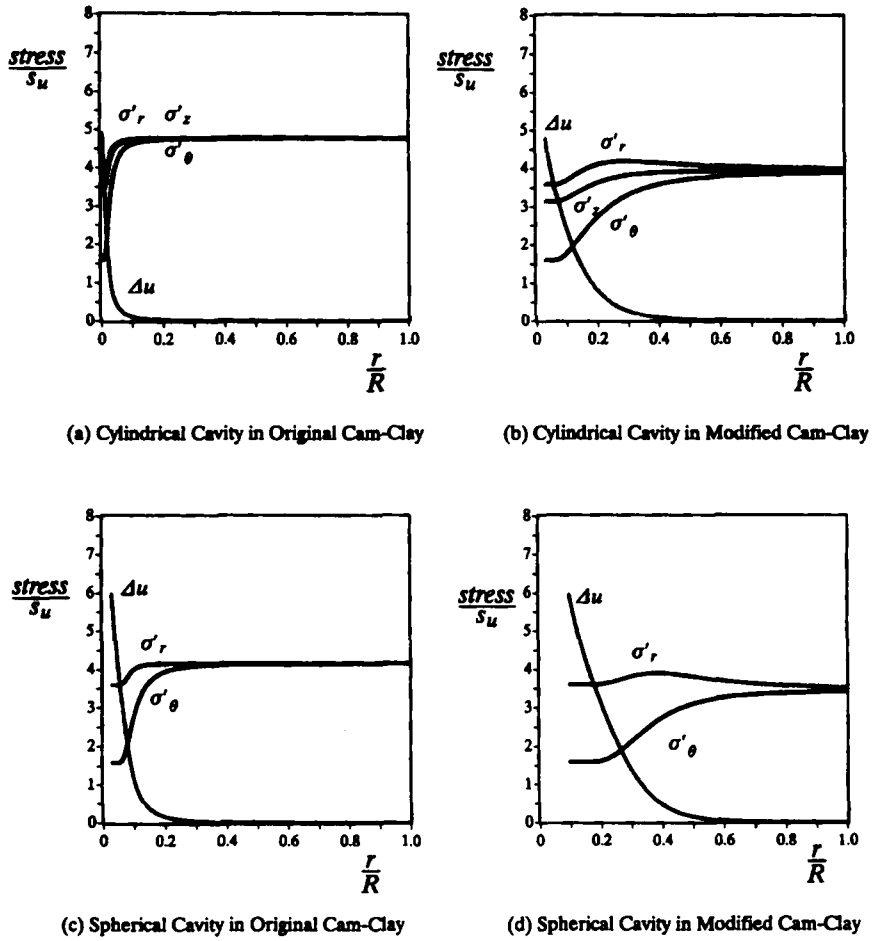

Figure 7. Stress distributions in plastic region for OCR of $n_p = 1{\cdot}001$

where $\dot{\delta}^e$ and $\dot{\gamma}^e$ represent the elastic volumetric and shear strain rates, respectively; $\mathring{\bar{p}}'$ and $\mathring{\bar{q}}$ are the material rates of change of the non-dimensional, effective mean and shear stress invariants. The instantaneous bulk and shear moduli are both functions of the specific volume v and mean effective pressure p' in general, so that the elastic stress–strain relation obtained by integration will be non-linear. The symbol $(\circ)$ denotes the material time derivative associated with a given solid material particle and it is related to the local time derivative $(\dot{})$, evaluated at fixed position r, by

$$(\circ) = (\dot{}) + w\frac{\partial(\ )}{\partial r} \tag{15}$$

where w is the radial speed of a solid material element.

In the initial, purely elastic phase of an undrained expansion the elastic volumetric strain rate $\dot{\delta}^e = 0$, so that from equation (14) the effective mean pressure remains constant and is equal to its initial value p'_0. The instantaneous elastic bulk and shear moduli hence also remain constant and equal to their initial values K_0 and G_0, respectively. The second part of equation (14) for the elastic shear strain rate can be integrated along a particle path, so that the shear stress invariant

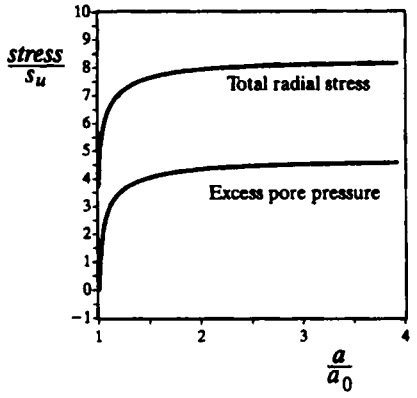

(a) Cylindrical Cavity in Original Cam-Clay

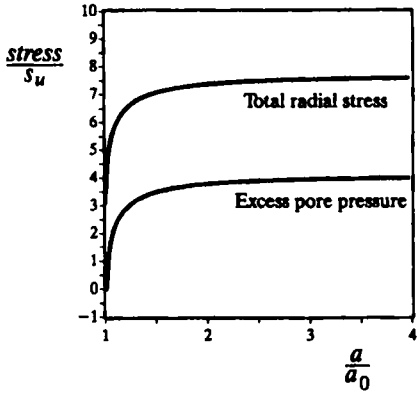

(b) Cylindrical Cavity in Modified Cam-Clay

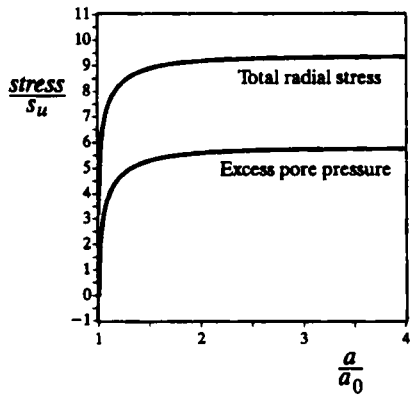

(c) Spherical Cavity in Original Cam-Clay

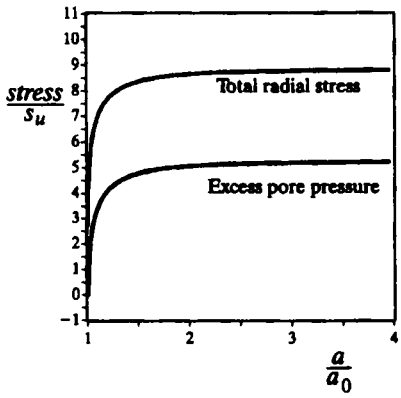

(d) Spherical Cavity in Modified Cam-Clay

Figure 8. Cavity expansion curves for OCR of $n_p = 1{\cdot}5$

q is just twice the initial elastic shear modulus times the finite shear strain γ, viz:

$$\gamma = \frac{\bar{q}}{2\bar{G}_0} \tag{16}$$

The radial and circumferential components of effective stress are hence given by

$$\bar{\sigma}'_r = \bar{p}'_0 + \frac{2\bar{G}_0\gamma k}{k+1} \quad \text{and} \quad \bar{\sigma}'_\theta = \bar{p}'_0 - \frac{2\bar{G}_0\gamma}{k+1} \tag{17}$$

These stresses can now be expressed in terms of the radial position coordinates by eliminating γ using either (8) or (9). It is to be emphasized that these effective stress distributions have been found without reference to the equilibrium equations and without the need to make any small strain assumptions. Since the effective mean pressure is constant the stress path of a material element in this elastic phase of the expansion is a vertical line in the $\bar{q}$–$\bar{p}'$ diagram (Figure 2).

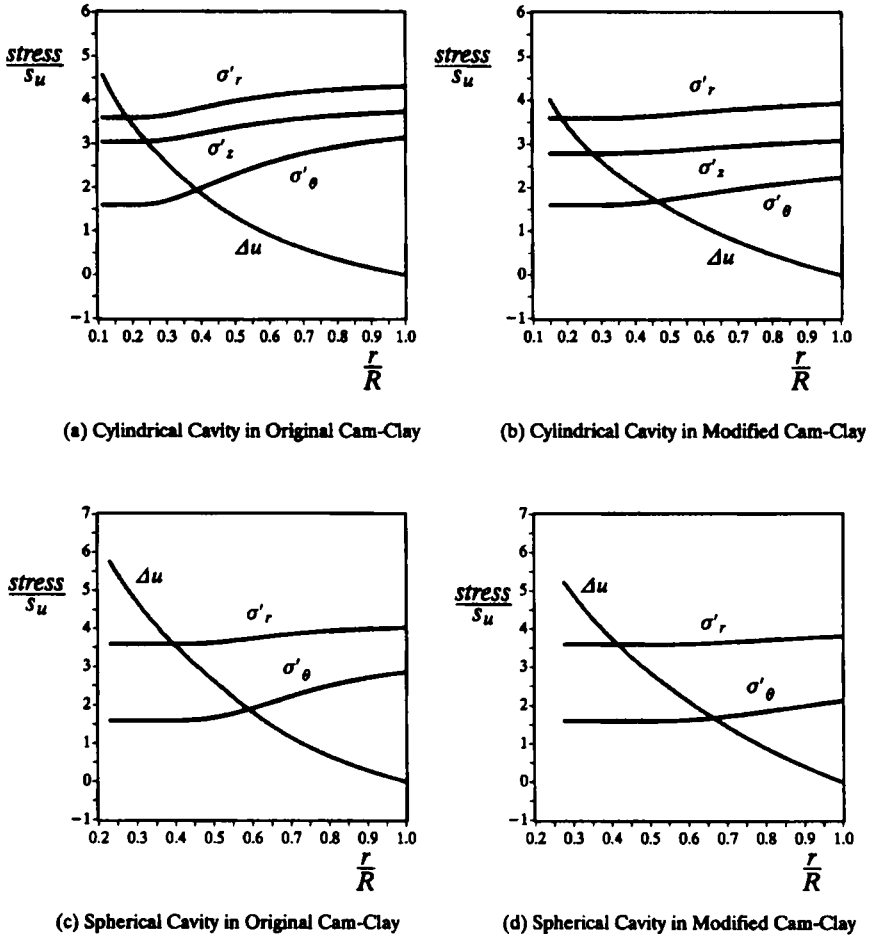

Figure 9. Stress distributions in plastic region for OCR of $n_p = 1{\cdot}5$

The soil first goes plastic at the cavity wall, when the shear stress invariant reaches the yield value q_0, which will depend upon the particular yield criterion. The corresponding shear strain is

$$\gamma_0 = (k+1)\ln\frac{a_1}{a_0} = \frac{\bar{q}_0}{2\bar{G}_0} = \frac{q_0}{2G_0} \tag{18}$$

where a_1 is the cavity radius at the onset of yielding, γ_0 is the shear strain to yield and is a measure of the compliance of the material. In a perfectly plastic model q_0 is twice the undrained shear stregnth so that γ_0 is the reciprocal of the rigidity index. This is not true in the more general models.

These results are also valid in the outer elastic region during the elastic–plastic phase of the expansion. The radius of the elastic/plastic boundary R at the instant when the cavity has radius a is given by

$$R^{k+1} = \frac{a^{k+1} - a_0^{k+1}}{1 - \exp(-\gamma_0)} \tag{19}$$

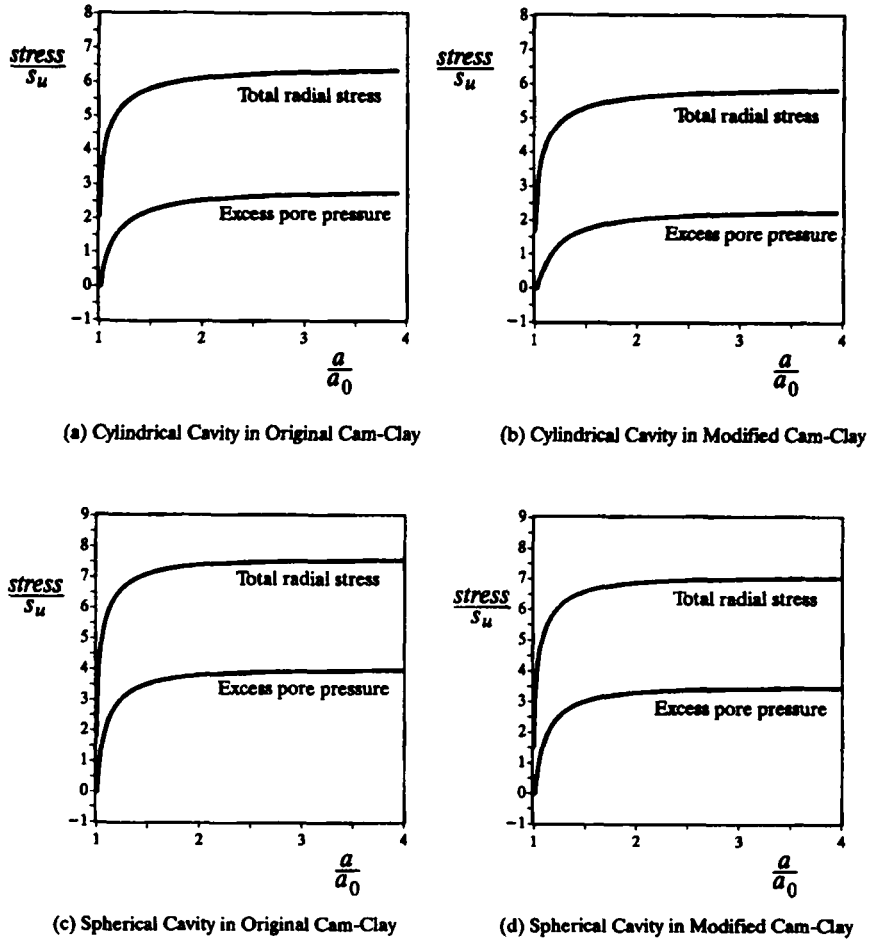

Figure 10. Cavity expansion curves for OCR of $n_p = 4$

using (9) or (10), so that this relation between the shear strain and radial co-ordinate can alternatively be written as

$$\left(\frac{r}{R}\right)^{k+1} = \frac{1 - \exp(-\gamma_0)}{1 - \exp(-\gamma)} \tag{20}$$

In the appendix, it is shown that the above solution can also be derived from the similarity solution for the expansion of a cavity with zero initial radius.

ELASTIC–PLASTIC PHASE OF EXPANSIONS

Effective stress distributions

Here the basic solution is developed in a general form appropriate to a wide class of materials, where the yield condition and flow rule can be written in the form:

$$\bar{q} = f(\bar{p}') \quad \text{and} \quad \frac{\dot{\delta}^p}{\dot{\gamma}^p} = g(\bar{p}') \tag{21}$$

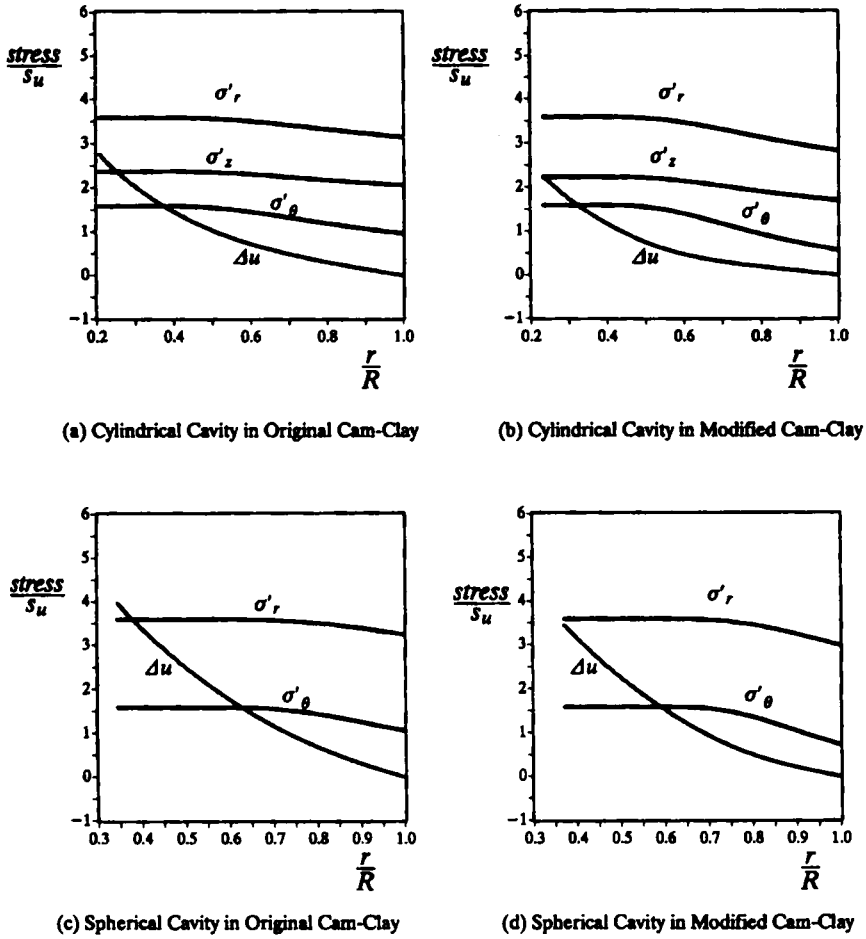

Figure 11. Stress distributions in plastic region for OCR of $n_p = 4$

In an undrained deformation the total volumetric strain-rate is zero, so that $\dot{\delta}^e = -\dot{\delta}^p$. It follows from (14) and (21) that the total strain-rate is

$$\dot{\gamma} = \dot{\gamma}^e + \dot{\gamma}^p = L(\bar{p}')\dot{\bar{p}}' \tag{22}$$

where

$$L(\bar{p}') = \frac{f'(\bar{p}')}{2\bar{G}(\bar{p}')} - \frac{1}{\bar{K}(\bar{p}')g(\bar{p}')} \tag{23}$$

Integrating (22) along a particle path starting at the elastic–plastic boundary gives a relation between the finite shear strain and the effective mean pressure:

$$\gamma = \gamma_0 + I(\bar{p}') - I(\bar{p}'_0) \tag{24}$$

where

$$I(\bar{p}') = \int^{\bar{p}'} L(\bar{p}')\,\mathrm{d}\bar{p}'. \tag{25}$$

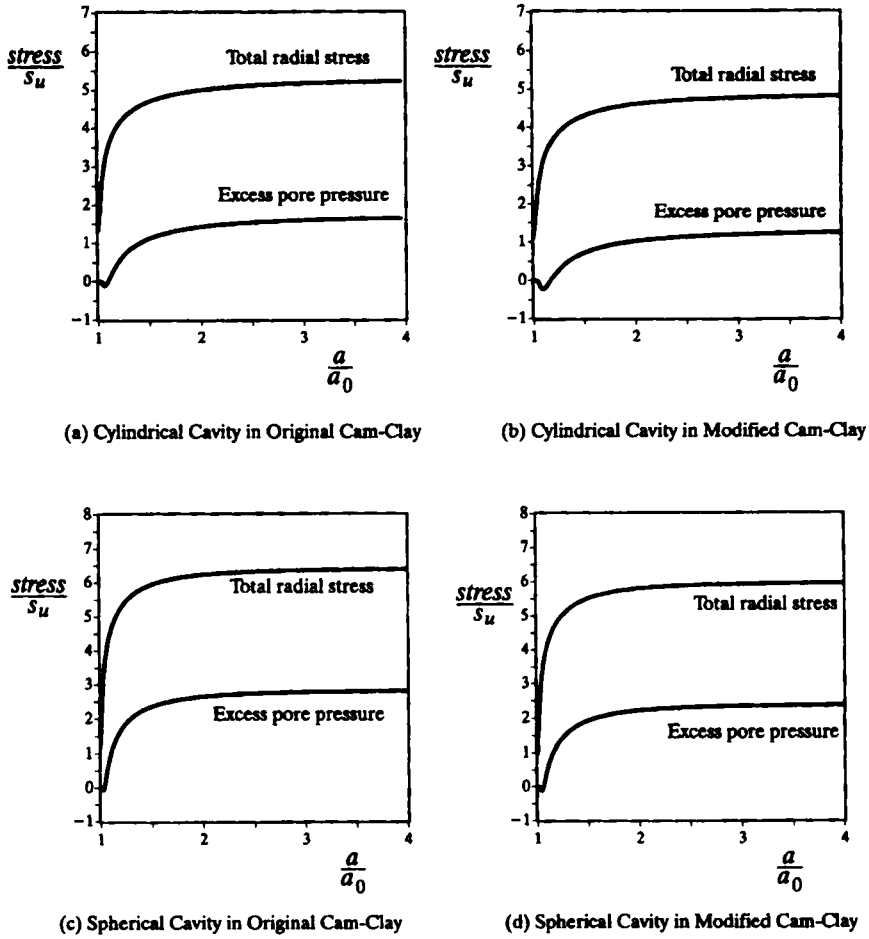

(a) Cylindrical Cavity in Original Cam-Clay

(b) Cylindrical Cavity in Modified Cam-Clay

(c) Spherical Cavity in Original Cam-Clay

(d) Spherical Cavity in Modified Cam-Clay

Figure 12. Cavity expansion curves for OCR of $n_p = 8$

As a special case, (24) describes the relationship between the cavity pressure and the cavity shear strain after the cavity wall becomes plastic. As will be shown in a later section the integral (25) can be evaluated analytically for the original Cam-Clay model and is readily evaluated numerically in other cases. The variation of $\bar{p}'$ with radius r can be obtained implicitly by eliminating γ between (24) and (8), (9) or (20).

Calculation of excess pore pressures

The distribution of pore pressure $u(r)$ can be calculated from the quasi-static radial equilibrium equation:

$$\frac{d\bar{\sigma}_r}{dr} + k\frac{\bar{\sigma}_r - \bar{\sigma}_\theta}{r} = 0 \tag{26}$$

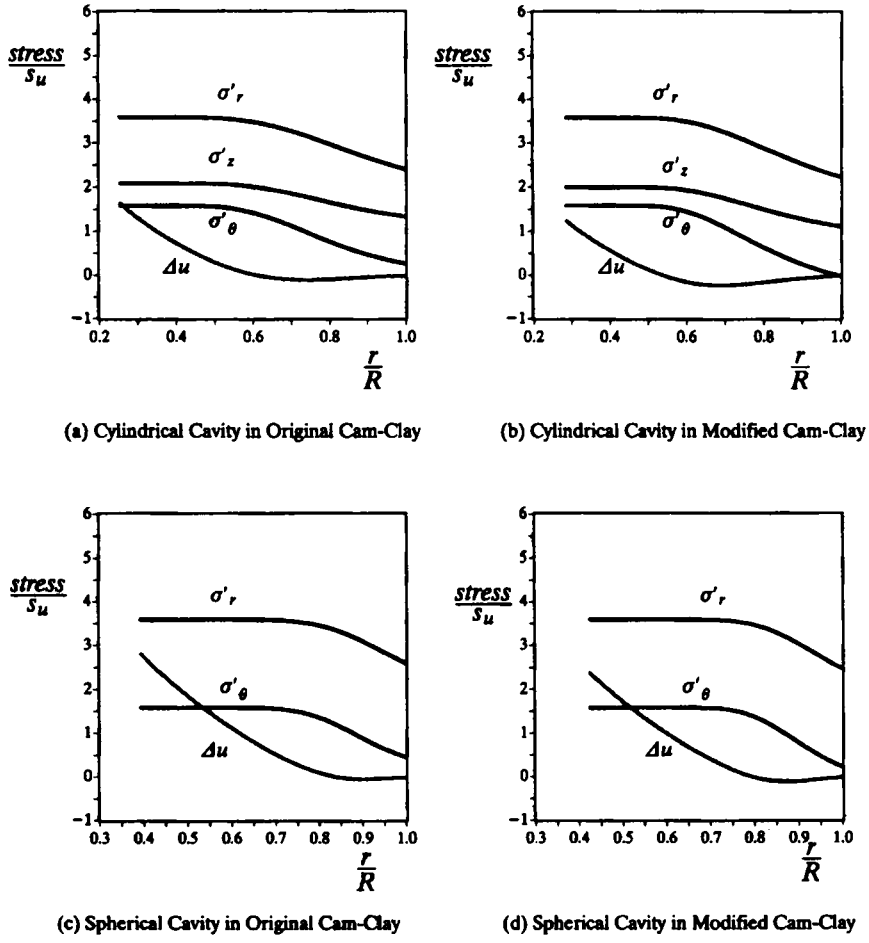

Figure 13. Stress distributions in plastic region for OCR of $n_r = 8$

Since $\bar{\sigma}_r = \bar{p} + (k/(k+1))\bar{q}$ and $\bar{p} = \bar{u} + \bar{p}'$, the non-dimensional pore pressure gradient is given by

$$\frac{d\bar{u}}{dr} = -\frac{d\bar{p}'}{dr} - \frac{k}{k+1}\frac{d\bar{q}}{dr} - \frac{k\bar{q}}{r} \tag{27}$$

Since the effective mean stress distribution is constant in the elastic region, the change in the pore pressure (i.e. excess pore pressure) in the elastic zone is given by

$$\Delta\bar{u} = -\frac{k}{k+1}\bar{q} - k\int \bar{q}\frac{dr}{r} \tag{28}$$

But $\bar{q}$ and (dr/r) can be expressed in terms of γ from (16) and the second equation of (11), so that (28) becomes

$$\Delta\bar{u} = -\frac{2k\bar{G}_0}{k+1}\left[\gamma - \int_0^\gamma \frac{\gamma}{\exp(\gamma) - 1}d\gamma\right] \doteq -\frac{k\bar{G}_0\gamma^2}{2(k+1)} \tag{29}$$

to second order in γ.

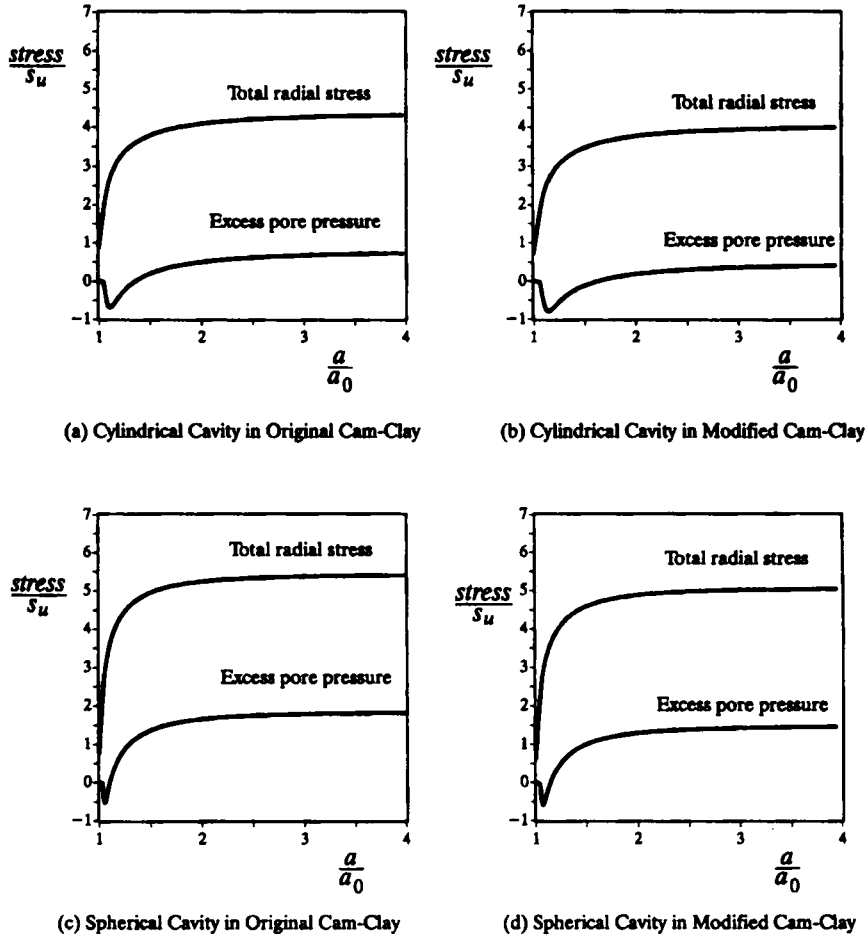

Figure 14. Cavity expansion curves for OCR of $n_p = 16$

The excess pore pressure is hence constant in the elastic region to first order in the shear strain as already noted by Collins and Stimpson.[17] To second order in strain, the excess pore pressure at the elastic–plastic boundary is

$$\Delta\bar{u}_0 = -\frac{k\bar{G}_0\gamma_0^2}{2(k+1)} \tag{30}$$

Excess pore pressures in plastic regions

Integrating (27) through the plastic region from the elastic/plastic boundary yields a relation between the excess pore pressure and the finite shear strain:

$$\Delta\bar{u} = \Delta\bar{u}_0 - (\bar{p}' - \bar{p}'_0) - \frac{k}{k+1}(\bar{q} - \bar{q}_0 - (J(\gamma) - J(\gamma_0))) \tag{31}$$

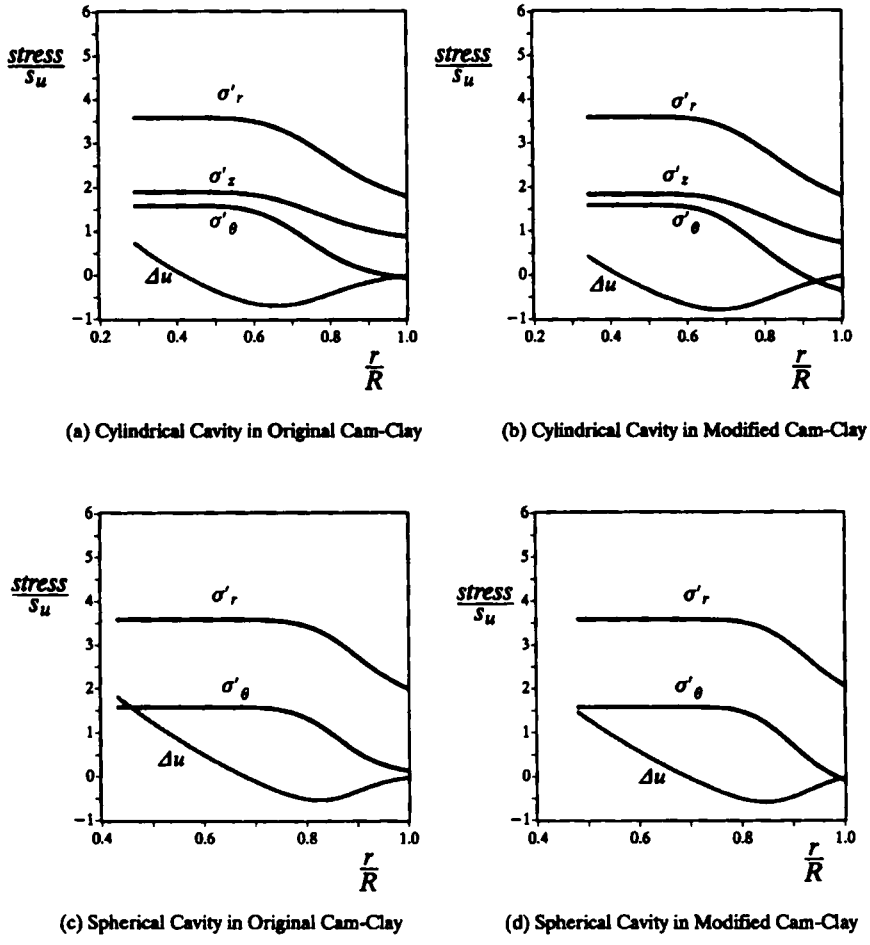

Figure 15. Stress distributions in plastic region for OCR of $n_p = 16$

where the integral J is most conveniently evaluated numerically by expressing both $\bar{q}$ and r in terms of $\bar{p}'$ using (11), (21) and (22):

$$J(\gamma) = \int^{\gamma} \frac{\bar{q}}{(\exp(\gamma) - 1)} d\gamma = \int^{\gamma} \frac{f(\bar{p}')L(\bar{p}')}{\exp(\gamma) - 1} d\bar{p}' \tag{32}$$

Again, as a special case, (31) represents the plastic relationship between the excess pore pressure and the finite shear strain for the cavity wall. Once the effective stress state has essentially reached the critical state, the value of $\bar{q}$ is effectively constant and (32) can then be integrated analytically to give

$$J(\gamma) \doteq \bar{q}_{cs} \ln(1 - \exp(-\gamma)) \tag{33}$$

PERFECTLY PLASTIC MODEL

Before discussing the solutions for various critical state models it is instructive to firstly review the solution for a perfectly plastic model, yielding being governed by the Tresca criterion. This

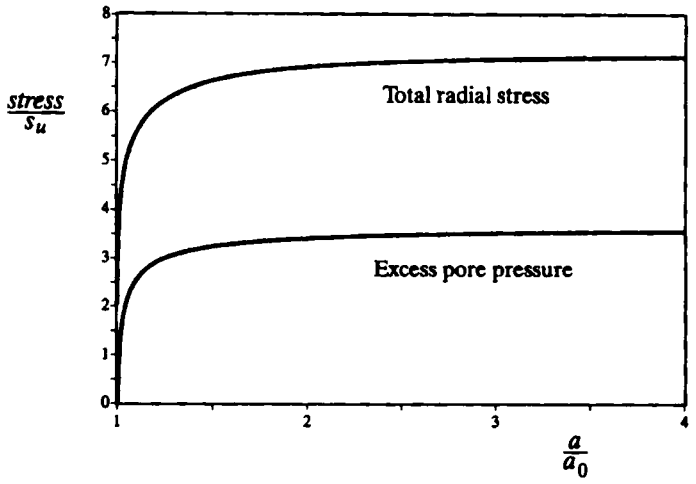

(a) Cylindrical Cavity with the Hvorslev yield surface

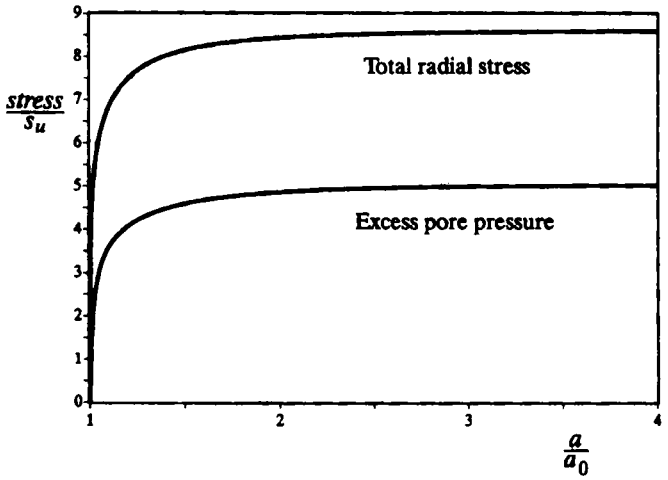

(b) Spherical Cavity with the Hvorslev yield surface

Figure 16. Cavity expansion curves derived from the original Cam-Clay–Hvorslev yield criterion for OCR of $n_p = 4$

corresponds to the situation where the in situ soil is already at the critical state. Since the shear stress and effective mean pressure are now constant through the plastic annulus the J integral in (32) can be evaluated analytically, giving:

$$\Delta\bar{u} = \Delta\bar{u}_0 + \frac{k}{k+1}\bar{q}_0 \ln\frac{1-\exp(-\gamma)}{1-\exp(-\gamma_0)} \tag{34}$$

or, in terms of the radial co-ordinate

$$\Delta\bar{u} = \Delta\bar{u}_0 + k\bar{q}_0 \ln\frac{R}{r} = \Delta\bar{u}_0 + \frac{k}{k+1}\bar{q}_0 \ln\frac{(\frac{a}{r})^{k+1} - (\frac{a_0}{r})^{k+1}}{1-\exp(-\gamma_0)} \tag{35}$$

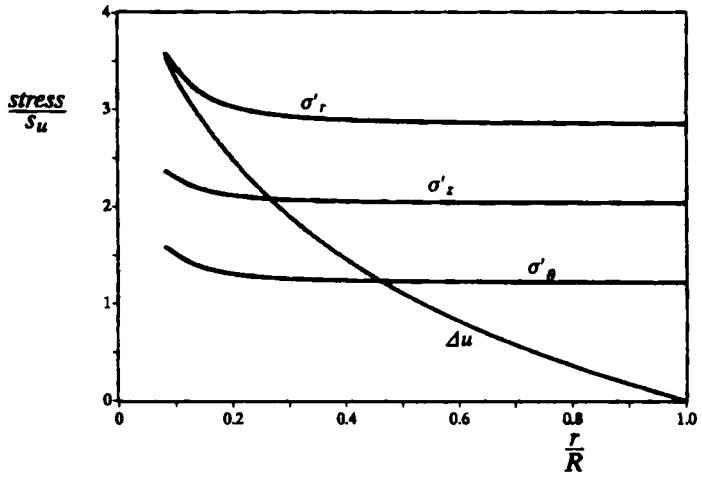

(a) Cylindrical Cavity with the Hvorslev yield surface

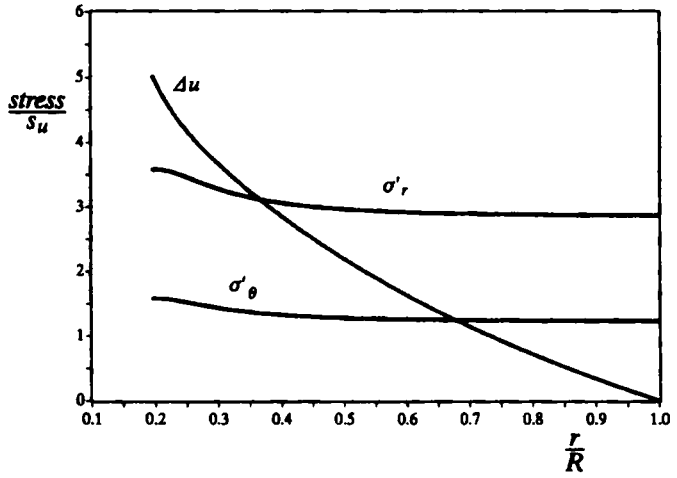

(b) Spherical Cavity with the Hvorslev yield surface

Figure 17. Stress distributions derived from the original Cam-Clay–Hvorslev yield criterion foir OCR of $n_p = 4$

using (19) and (20). To first order in the elastic limit strain γ_0 the excess pore pressure at the cavity wall is

$$\Delta\bar{u}_c \doteq \frac{k}{k+1}\bar{q}_0\left[\ln\left(1-\left(\frac{a_0}{a}\right)^{k+1}\right)+\ln I_r\right] \tag{36}$$

where $I_r = 1/\gamma_0$ is the well-known rigidity index. Using the above equation, the well-known total radial stress solution at the cavity wall derived by Gibson and Anderson[2] is recovered:

$$\bar{\sigma}_r|_c = \bar{p}_0 + \frac{k}{k+1}\bar{q}_0\left[1+\ln\left(1-\left(\frac{a_0}{a}\right)^{k+1}\right)+\ln I_r\right] \tag{37}$$

In the initial stages of the deformation, where γ is small, (36) reduces to

$$\Delta\bar{u}_c \doteq \frac{k}{k+1}\bar{q}_0[\ln\gamma_c + \ln I_r] \tag{38}$$

showing that in the early phases of the expansion the excess pore pressure is proportional to the logarithm of the cavity shear strain. On the other hand, for large expansions $a_0/a \to 0$, we have

$$\Delta\bar{u}_c \doteq \frac{k}{k+1}\bar{q}_0 \ln I_r \tag{39}$$

$$\bar{\sigma}_r|_c = \bar{p}_0 + \frac{k}{k+1}\bar{q}_0(1 + \ln I_r) \tag{40}$$

which are the well-known limiting solutions for the excess pore pressure and the total cavity pressure in a cavity expanding from zero initial radius in the perfectly plastic material.

CRITICAL STATE PLASTICITY MODELS

The original Cam-Clay model for both normally and overconsolidated clays

The yield function in the original Cam-Clay model proposed by Schofield and Wroth[21] is

$$\bar{q} = f(\bar{p}') = -\frac{M}{\Lambda}\bar{p}'\ln\bar{p}' \tag{41}$$

where the stresses have been non-dimensionalised by the equivalent consolidation pressure at the same specific volume v:

$$p'_e = \exp\left(\frac{N - v}{\lambda}\right) \tag{42}$$

The constant $\Lambda = 1 - \kappa/\lambda$, where κ, λ are the slopes of the elastic swelling line and normal consolidation line, respectively, in $\ln p' - v$ space and N is the value of v on the normal consolidation line when $p' = 1$ kPa. The final critical state constant M is the slope of the critical state line in $\bar{p}' - \bar{q}$ space.

In this model the elastic moduli are given by

$$\bar{K} = \frac{v\bar{p}'}{\kappa} \quad \text{and} \quad \bar{G} = \alpha\bar{K} \tag{43}$$

where $\alpha = (1 + k)(1 - 2\mu)/(2(1 + (k - 1)\mu))$ and μ denotes Poisson's ratio. Some authors assume μ to be constant whilst others keep G fixed and use (43) to calculate the Poisson's ratio (see References 22 and 23). In the present context it proves advantageous to assume a constant value of the Poisson's ratio, since then all the material parameters defining the model are dimensionless, which results in a number of simplifying scaling laws. Nevertheless, it will be demonstrated in the next section that a constant shear modulus can also be included in the present cavity expansion solution procedure.

The overconsolidation ratio (OCR) in terms of the mean effective stress is

$$n_p = (\bar{p}'_0)^{-1/\Lambda} \tag{44}$$

At the critical state $\bar{q}/\bar{p}' = M$, $n_p = e$ and $\bar{p}' = e^{-\Lambda}$, whilst the undrained stress path in $\bar{p}' - \bar{q}$ space has a maximum value when $\bar{p}' = 1/e$ and $\bar{q}/\bar{p}' = M/\Lambda$ as shown in Figure 3.

The ratio of the plastic volumetric and shear strain rates calculated from the normal flow rule is

$$\frac{\dot{\delta}^p}{\dot{\gamma}^p} = g(\bar{p}') = \frac{kM}{(k+1)\Lambda}(\Lambda + \ln \bar{p}') \tag{45}$$

The function $L(\bar{p}')$ needed to calculate the effective pressure distributions in (23) is, hence,

$$L(\bar{p}') = -\frac{A(1+\ln \bar{p}')}{\bar{p}'} - \frac{B}{\bar{p}'(\Lambda + \ln \bar{p}')} \tag{46}$$

and upon integration the function needed in (24) to calculate the shear strain is

$$I(\bar{p}') = -A(\ln \bar{p}' + \tfrac{1}{2}(\ln \bar{p}')^2) - B \ln|(\Lambda + \ln \bar{p}')| \tag{47}$$

where $A = M\kappa/(2\Lambda\alpha v)$ and $B = (k+1)\Lambda\kappa/(kMv)$ are constants. Note that the value of the integral I and hence the shear strain is inversely proportional to the specific volume v.

The original Cam-Clay model for normally consolidated and lightly overconsolidated clays—the Hvorslev yield surface for heavily overconsolidated clays

It is well established that for overconsolidated clays, the original Cam-Clay yield criterion tends to overpredict the soil strength significantly. In this region, the Hvorslev surface has often been used as the yield function. The Hvorslev yield surface is a straight line in $\bar{p}' - \bar{q}$ space (see Reference 22):

$$\bar{q} = h\bar{p}' + (M - h)\exp(-\Lambda) \tag{48}$$

where h is the slope of the Hvorslev yield surface, Figure 4.

It is also noticed that the use of (43) for heavily overconsolidated clays would result in unrealistically low values of the elastic moduli. To overcome this shortcoming, Randolph *et al.*[13] proposed a more realistic hypothesis that is to select G as half of the maximum value of the elastic bulk modulus, K_{max} that was ever reached during the history of the soil. In their proposal, the bulk modulus is still assumed to be pressure dependent, and so the resulting model is conservative for elastic behaviour (see Reference 24). Equation (43) is hence replaced by the following expression for heavily overconsolidated clays:

$$\bar{K} = \frac{v\bar{p}'}{\kappa} \quad \text{and} \quad \bar{G} = \frac{v + \lambda(\Lambda - 1)\ln n_p}{2\kappa}(n_p)^{1-\Lambda} \tag{49}$$

Using (48) as the yield function, (41) as the plastic potential and (49) for the elastic moduli, we can obtain

$$L(\bar{p}') = \frac{h}{2\bar{G}} - \frac{(1+k)\kappa}{kv(M-h)}\frac{1}{(\bar{p}' - \exp(-\Lambda))} \tag{50}$$

and

$$I(\bar{p}') = \frac{h\bar{p}'}{2\bar{G}} - \frac{(1+k)\kappa}{kv(M-h)}\ln(\bar{p}' - \exp(-\Lambda)) \tag{51}$$

where the constant $\bar{G}$ is given by equation (49).

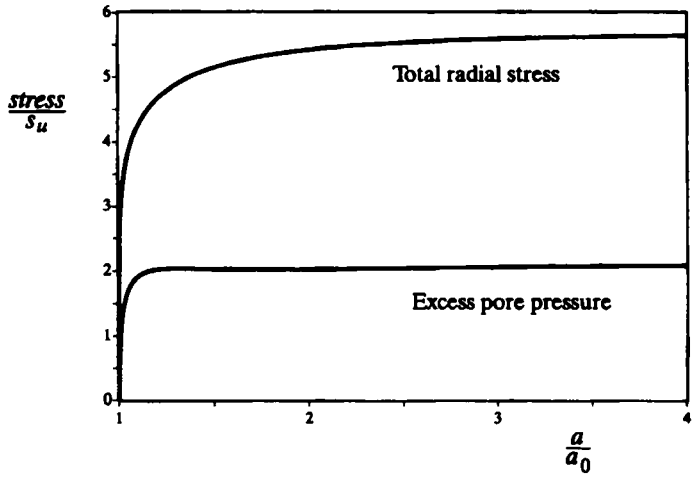

(a) Cylindrical Cavity with the Hvorslev yield surface

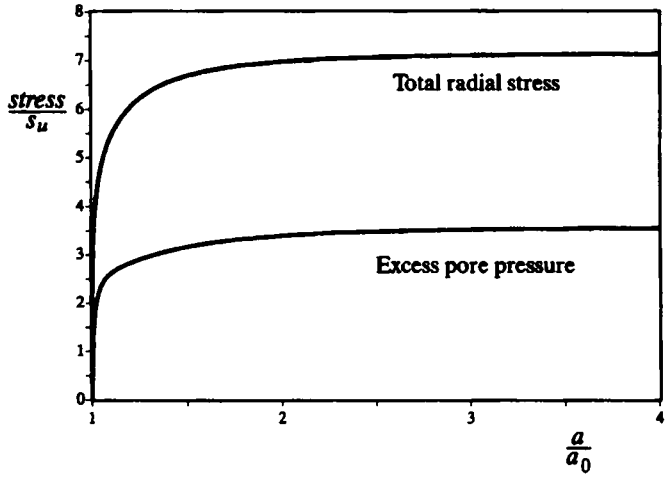

(b) Spherical Cavity with the Hvorslev yield surface

Figure 18. Cavity expansion curves derived from the original Cam-Clay–Hvorslev yield criterion for OCR of $n_p = 8$

The modified Cam-Clay model for both normally and overconsolidated clays

The yield function in the modified Cam-Clay model (Muir Wood[23]) is

$$\bar{q} = f(\bar{p}') = M\bar{p}'\sqrt{(\bar{p}'^{-1/\Lambda} - 1)} \tag{52}$$

At the critical state $\bar{q}/\bar{p}' = M$, $n_p = 2$ and $\bar{p}' = 2^{-\Lambda}$, as shown in Figure 5.

The ratio of the plastic volumetric and shear strain rates calculated from the normal flow rule is

$$\frac{\dot{\delta}^p}{\dot{\gamma}^p} = g(\bar{p}') = -\frac{kM}{2(k+1)}\frac{\bar{p}'^{-1/\Lambda}}{(\bar{p}'^{-1/\Lambda} - 1)^{1/2}} \tag{53}$$

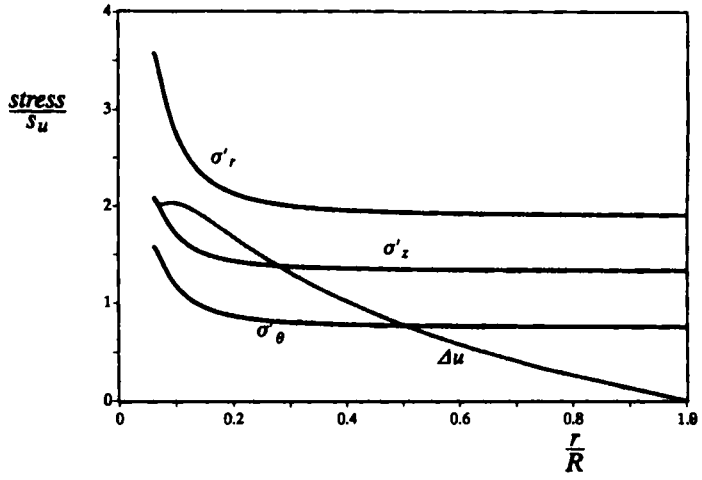

(a) Cylindrical Cavity with the Hvorslev yield surface

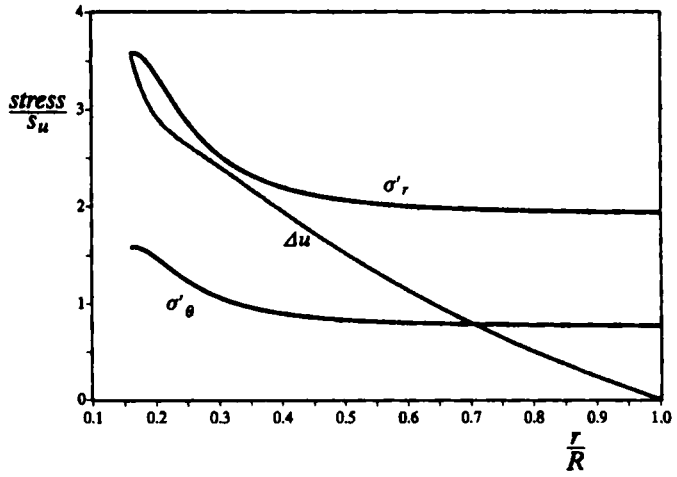

(b) Spherical Cavity with the Hvorslev yield surface

Figure 19. Stress distributions derived from the original Cam-Clay–Hvorslev yield criterion foir OCR of $n_p = 8$

The function $L(\bar{p}')$ needed to calculate the effective pressure distributions in (23) can be obtained by using (52) and (53). Unlike the original Cam-Clay model, the function needed in (24) to calculate the shear strain for the modified Cam-Clay model can not be obtained in a closed form and instead a simple numerical integration must be used.

RESULTS AND DISCUSSION

In this section some results for the cavity expansion curves and stress distributions for the undrained cavity expansion in soils with various critical state models are presented. The values of the critical state parameters chosen for the examples presented here are those relevant for London clay: $\Gamma = 2{\cdot}759$, $\lambda = 0{\cdot}161$, $\kappa = 0{\cdot}062$, the critical state friction angle $\phi'_{cs} = 22{\cdot}75°$ and the Hvorslev friction angle $\phi'_{hc} = 19{\cdot}7°$ (see References 22 and 23). All the results presented are for the case

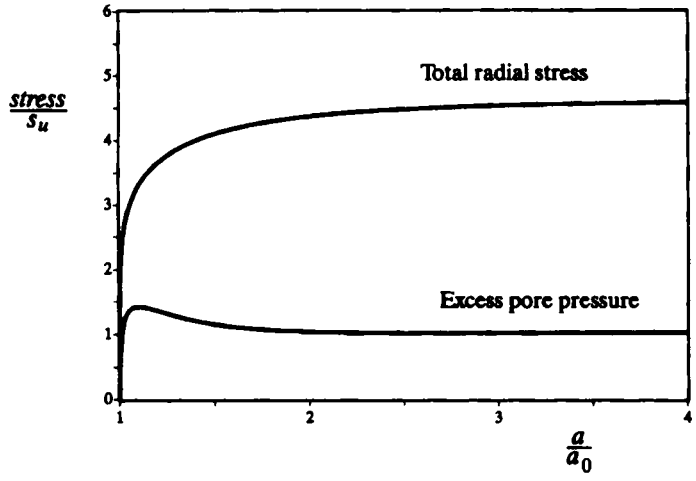

(a) Cylindrical Cavity with the Hvorslev yield surface

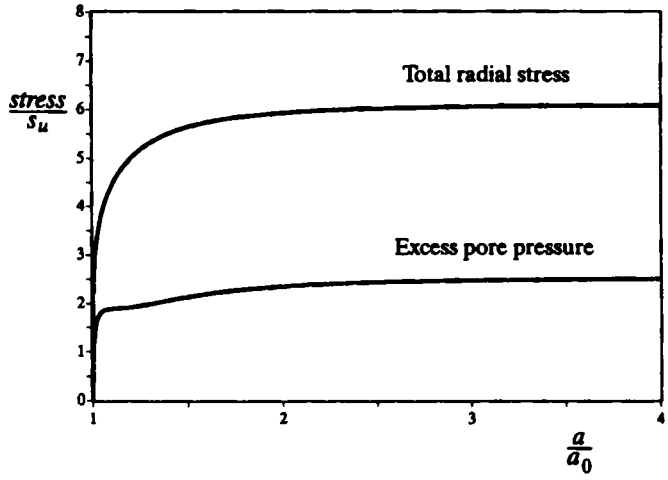

(b) Spherical Cavity with the Hvorslev yield surface

Figure 20. Cavity expansion curves derived from the original Cam-Clay–Hvorslev yield criterion for OCR of $n_p = 16$

when the specific volume of the soil v is equal to 2·0. The Poisson's ratio μ is assumed to be 0·3 for all the calculations when the original and modified Cam-Clay models are used. If the critical state friction angle of the soil is assumed to be the same for both the triaxial and plane strain loading conditions (see Muir Wood,[23] p. 178 for experimental evidence and further discussion), the values of M for both spherical and cylindrical cavities can be determined using $M = 6\sin\phi'_{cs}/(3 - \sin\phi'_{cs})$ and $M = 2\sin\phi'_{cs}$, respectively. Similar expressions can be used to determine h from ϕ'_{hc}. Following Yu and Houlsby,[10] the vertical effective stress σ'_z for the cylindrical case can be obtained from the other two stress components by using the plane strain condition in the vertical direction. This condition therefore requires the elastic vertical strain rate to be zero since equations (13) and (21) together with the plastic flow rule imply that the plastic vertical strain rates are zero.

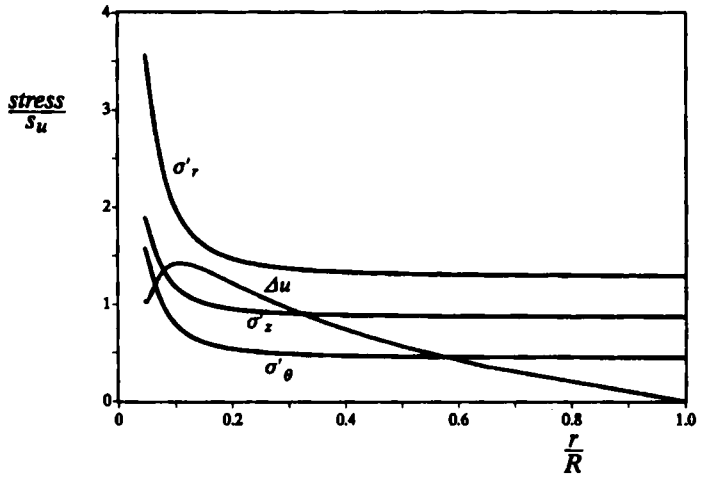

(a) Cylindrical Cavity with the Hvorslev yield surface

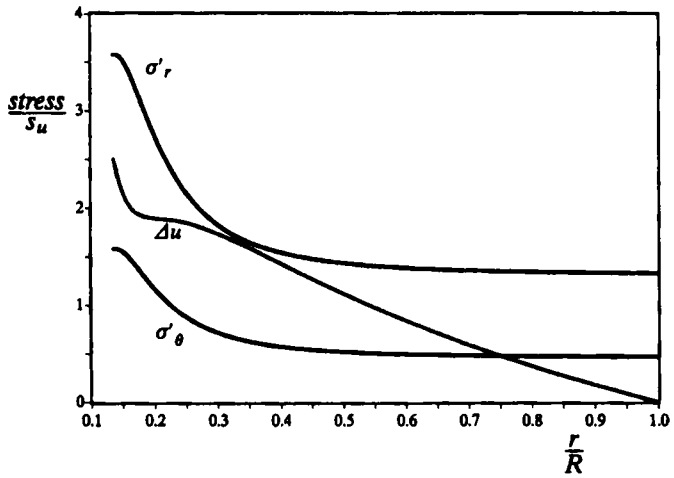

(b) Spherical Cavity with the Hvorslev yield surface

Figure 21. Stress distributions derived from the original Cam-Clay–Hvorslev yield criterion foir OCR of $n_p = 16$

The first set of results is obtained with the original Cam-Clay and the modified Cam-Clay models. Results showing the cavity expansion curve and stress distribution in the plastically deformed region at the instant of $a/a_0 = 4$ for the overconsolidation ratios of $n_p = 1{\cdot}001, 1{\cdot}5, 4, 8, 16$ are presented in Figures 6–15. Both spherical and cylindrical cases have been included. The reason for using $n_p = 1{\cdot}001$ to represent a normally consolidated clay is that when $n_p = 1$ the shear strain required to reach the yield surface is zero and from equation (19) the radius of the elastic–plastic boundary becomes indeterminate. All the stresses and pressures have been normalised by the undrained shear strength of the soil which is defined by $s_u = 0{\cdot}5M\exp((\Gamma - v)/\lambda)$. *It should also be stressed that the total radial stress values presented in this section do not include ambient pore pressure.* As far as the cavity expansion curves are concerned, it is interesting to note that the responses of the modified Cam-Clay and the original Cam-Clay are similar for normally

consolidated clays. For overconsolidated soils, the cavity expansion curves predicted by the original Cam-Clay model are slightly stiffer than those from the modified Cam-Clay model. In particular, the limit solutions of the total cavity pressure and the excess pore pressure predicted by the modified Cam-Clay model are typically 10–20 per cent smaller than those obtained with the original Cam-Clay model. With reference to the stress distributions, it is found that the radius of the elastic–plastic boundary calculated with the original Cam-Clay model is much greater than that from the modified Cam-Clay model. This is because that the shear strain required to reach the modified Cam-Clay yield surface γ_0 is greater than that required to reach the original Cam-Clay yield surface. It is also found that when the overconsolidation ratio increases, the excess pore pressure could become negative and this is mainly due to the fact that very low elastic moduli are obtained from (43) for heavily overconsolidated clays.

The second set of results is for heavily overconsolidated clays modelled by the Hvorslev yield surface with a constant shear modulus. Results showing cavity expansion curve and stress distribution in the plastic region at the instant of $a/a_0 = 4$ for the overconsolidation ratios of $n_p = 4, 8, 16$ are presented in Figures 16–21. A comparison between the results from the Hvorslev yield criterion and those of the original and modified Cam-Clay models indicates that the limit solutions of the total cavity pressure and the excess pore pressure derived from the Hvorslev yield criterion are slightly higher than those from the original and modified Cam-Clay models, but this difference tends to decrease with the increase of the overconsolidation ratio. It is also noted that the radius of the elastic–plastic boundary calculated with the Hvorslev model is much greater than those from both the original and modified Cam-Clay models. Unlike the original and modified Cam-Clay models, no negative excess pore pressures have been observed in the results of the Hvorslev yield criterion when the overconsolidation ratio is less than 16; this is because a constant shear modulus has been used in the Hvorslev model.

In summary, it may be concluded that the choice of a particular critical state model seems to have a more pronounced effect on the results for excess pore pressures, effective stress distributions and the size of the plastically deformed region than it does on the total cavity pressures.

Prediction of excess pore pressures during pile installation in overconsolidated clays

Over the last three decades, many investigators (see Reference 25 for details) have measured pore water pressures generated at the pile–soil interface during pile installation in clay soils. More high-quality experimental research on pile testing has been carried out in recent years and notable examples include the work carried out at Oxford University by Coop and Wroth[26] and that of Bond and Jardine[27] at Imperical College.

The work of Coop and Wroth[26] on instrumented pile tests in both normally consolidated and heavily overconsolidated clays suggests that although the previous cavity expansion theories (e.g. Reference 13) may be satisfactorily used to model the installation of a displacement pile in normally consolidated clays, they do not seem to be able to predict the pile behaviour in a heavily overconsolidated clay. In particular, Coop and Wroth[26] noted that the excess pore pressures predicted by the cavity expansion theory of Randolph *et al.*[13] for pile installation in high OCR clays are much higher than those measured in the instrumented pile testing. This finding has been confirmed by an independent research programme of Bond and Jardine[27] on pile testing in a heavily overconsolidated London clay. Using the cavity expansion theory of Randolph *et al.*,[13] Wroth *et al.*[28] have suggested that the normalized excess pore pressure (i.e. the excess pore pressure divided by initial undrained shear strength of the soil) for heavily overconsolidated London clay should be in the range of 3·1–3·6. However, the results from the instrumented pile tests in London clay indicate that negative pore pressures were recorded during the pile

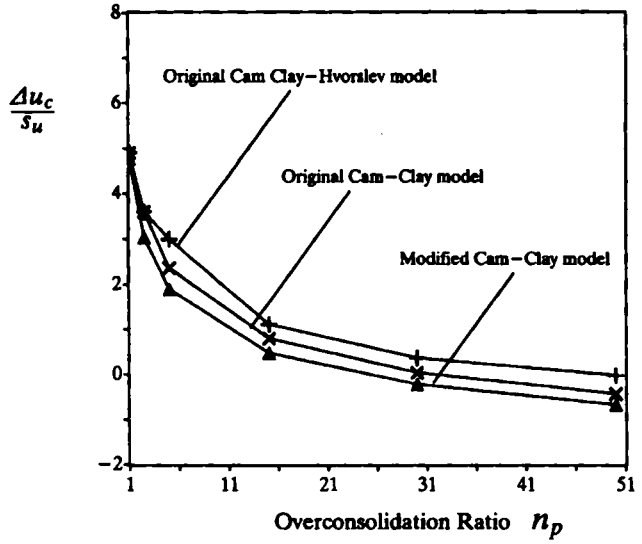

Figure 22. Variations of the normalised excess pore pressures at cavity wall with the overconsolidation ratio for initial specific volume of 2·0

installation. The relative insensitivity to overconsolidation ratio of the excess pore pressures, as predicted by the cavity expansion theory of Randolph *et al.*,[13] is probably largely due to a combined effect of their choices of variation of shear modulus G with overconsolidation ratio and the modified Cam-Clay yield surface for modelling heavily overconsolidated clays.

In an attempt to explain the negative excess pore pressures measured at the pile wall during the pile driving in high OCR clays, the present cavity expansion solutions are presented in such a way that the variations of the excess pore pressures with overconsolidation ratio can be studied in detail. The cavity expansion results for London clay predicted by three different critical state soil models when initial specific volume is equal to 2·0 are plotted in Figure 22 in terms of the normalized excess pore pressures at cavity wall against the overconsolidation ratio. The values of excess pore pressures are obtained at the instant of cavity expansion ratio $a/a_0 = 4$. It is interesting to see that, for all the soil models, the normalized excess pore pressures tend to decrese, in a similar manner, with the increase of the overconsolidation ratio. The theoretical trends shown in Figure 22 for the case when the overconsolidation ratio is less than 10 are confirmed by the field measurements reported by Kirby and Esrig.[25] According to Figure 22, the excess pore pressures could become negative if the overconsolidation ratio is greater than 25. As the overconsolidation ratio of London clay is in the range of 20 to 50,[27] the results in Figure 22 suggests that negative excess pore pressures could be generated at the pile wall during the pile installation in London clay. This is exactly what has been observbed by Bond and Jardine[27] in their experimental research on pile testing in London clay for which the specific volume of the soil is slightly less than 2·0.

To check if the specific volume of soils will have any influence on the variation of the normalized excess pore pressure with the overconsolidation ratio, results for three different initial specific volumes are presented in Figure 23. It is found that the normalized excess pore pressure for a given overconsolidation ratio increases slightly with the increase of the initial specific volume of the soil.

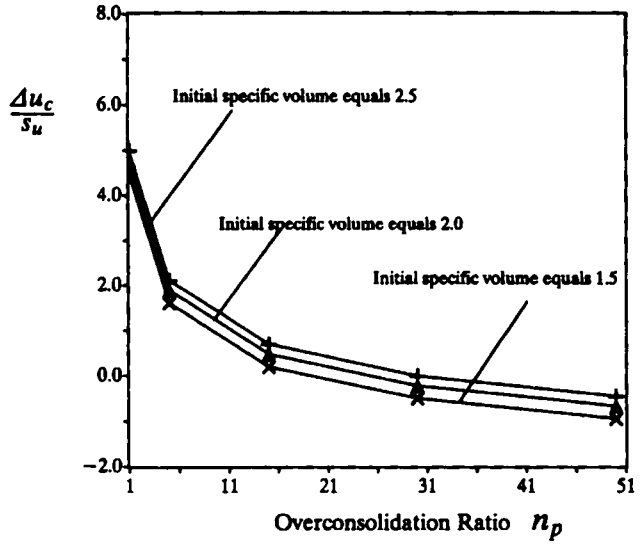

Figure 23. Variations of the normalised excess pore pressures at cavity wall with the overconsolidation ratio at various initial specific volumes predicted by the modified Cam-Clay model

CONCLUSIONS

This paper presents an analytical study of the undrained expansion of cylindrical and spherical cavities in soil with various critical state soil models. The solution procedure is applicable to large strain cavity expansions in any isotropically hardening materials. In all cases only simple quadratures are involved, but in the case of original Cam-Clay a complete analytical solution has been derived. It has also been shown that the well-known perfectly plastic solution can be recovered as a special case of the present solution. The influence of the choice of various critical state models on the cavity expansion behaviour has been investigated in detail by comparing the results of cavity expansion curves and stress distributions derived from different models. A brief application of the present cavity expansion solution to modelling of pile installation in cohesive soil confirms its potential and usefulness in geotechnical practice. The detailed application of the proposed solutions to pressuremeter analysis is beyond the scope of this paper and will be dealt with in future papers.

APPENDIX

Here it is demonstrated that once the similarity solution for the expansion of a cavity with zero initial radius (sometimes called the created problem) is known, the solution for any finite sized initial cavity can be deduced. Although this was pointed out long ago by Hill[29] (p. 115), this result does not seem to be well known. In the present context of hardening/softening soils, a number of similarity solutions have been found for cavity expansions in sand and clays.[14, 17]

The key feature of the created cavity expansion problem is that it does not possess a characteristic length. In consequence all the dependent variables (velocity, effective pressure, radial stress, excess pore pressure, etc.) depend only on the dimensionless ratio $\eta = r/R$, where r is the radial co-ordinate and R is the current radius of the elastic/plastic boundary. R is the 'time' variable which measures the progression of the expansion. For example, a typical variation with η of the dimensionless radial velocity $\bar{\omega} = \omega/\dot{R}$ is shown in Figure 24.

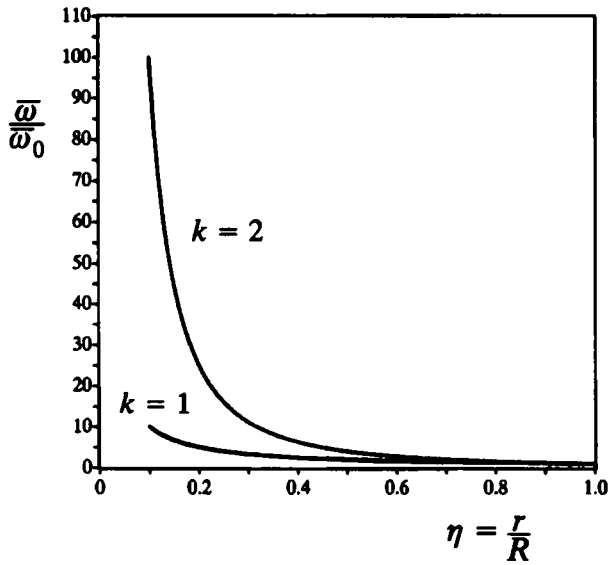

Figure 24. Typical variation with r/R of the dimensionless radial velocity $\bar{\omega}$

At the elastic/plastic boundary $\eta = 1$ and $\bar{\omega} = \bar{\omega}_0$ say, whilst at the cavity wall $r = c$ and η is constant, equal to η_c say. It is shown in Reference 17 that $\bar{\omega}$ is also equal to η_c at the cavity wall. For an undrained expansion at constant volume $\bar{\omega} = \bar{\omega}_0 \eta^{-k}$. No such simple relation exists for a drained expansion, and the velocity distribution $\bar{\omega}(\eta)$ must be found numerically.

Now consider the expansion of a cavity from the finite initial radius a_0. The cavity expands due to the pressure applied on its surface. The response will be the same when this pressure is applied due to the action of expanding soil in the cavity as when it is applied by some external agency provided the value of the pressure is the same. The solution for the finite cavity problem is hence just the same as that for the soil in the region $r \geqslant a_0$ in the created cavity problem.

At a generic instant we will denote the cavity radius by a, the radius of the elastic/plastic boundary by R and the radius of the corresponding created cavity by c, where $c/R = \eta_c$, a constant. In the initial phase $R < a$ and the deformation in $r > a$ is purely elastic. At the onset of plasticity, R and a have the same value a_1 say ($= a_0 \exp(\gamma_0)/(k + 1)$) in an undrained expansion, (18), and $c = c_1 = \eta_1 a_1$.

We put $\xi = a/R$ so at the onset of plastic flow $\xi = 1$. Since the cavity wall is a material surface $\dot{a} = \bar{\omega}(\xi)\dot{R}$; but also $\dot{a} = R\dot{\xi} + \dot{R}\xi$ obtained by differentiating $a = \xi R$. Elimination of $\dot{R}$ and integrating give

$$\ln\left(\frac{a}{a_1}\right) = \ln \xi + \int_1^{\xi} \frac{\mathrm{d}\xi}{\bar{\omega}(\xi) - \xi} \tag{54}$$

The dimensionless velocity $\bar{\omega}(\xi)$ is known from the similarity solution and hence this expression relates the cavity radius to the dimensionless parameter ξ ($= \eta$ in the similarity solution), and therefore the effective pressure, excess pore pressure, radial stress, etc. at the cavity wall can be deduced immediately from the similarity solution.

In the present case of undrained expansions $\bar{\omega} = \bar{\omega}_0 \eta^{-k}$ and (54) can be integrated to give

$$\zeta^{k+1} = \left(\frac{a}{R}\right)^{k+1} = \frac{1 - \exp(-\gamma_0)}{1 - \exp(-\gamma_c)} \tag{55}$$

which establishes equation (19) again. This technique is nevertheless most likely to be of use for drained problems, since the finite sized initial cavity problem under drained loading conditions is appreciably more difficult to analyse directly than is the corresponding undrained expansion.

REFERENCES

1. P. Chadwick, 'The quasi-static expansion of a spherical cavity in metals and ideal soils', *Q. J. Mech. Appl. Math.*, **12**, 52–71 (1959).
2. R. E. Gibson and W. F. Anderson, '*In situ* measurement of soil properties with the pressuremeter', *Civil Eng. Public Works Rev.* **56**, 615–618 (1961).
3. B. Ladanyi, 'Expansion of a cavity in a saturated medium', *J. Soil Mech. Found. Div. ASCE*, **89**, 127–161 (1963).
4. A. S. Vesic, 'Expansion of cavities in infinite soil mass', *J. Soil Mech. Found. Div. ASCE*, **98**, 265–290 (1972).
5. M. M. Baligh, 'Cavity expansion in sands with curved envelopes', *J. Soil Mech. Found. Div. ASCE*, **102**, 1131–1146 (1976).
6. J. O. M. Hughes, C. P. Wroth and D. Windle, 'Pressuremeter test in sands', *Geotechnique*, **27**, 455–477 (1977).
7. J. P. Carter, J. R. Booker and S. K. Yeung, 'Cavity expansion in cohesive-frictional soils', *Geotechnique*, **36**, 349–358 (1986).
8. D. Bigoni and F. Landuro, 'The quasi-static finite cavity expansion in a non standard elastoplastic medium', *Int. J. Mech Sci.*, **31**, 825–837 (1989).
9. H. S. Yu and G. T. Houlsby, 'Finite cavity expansion in dilatant soil: loading analysis' *Geotechnique*, **41**, 173–183 (1991).
10. H. S. Yu, 'Expansion of a thick cylinder of soils', *Comput. Geotechnics*, **14**, 21–41 (1992).
11. H. S. Yu and G. T. Houlsby, 'A large strain analytical solution for cavity contraction in dilatant soils', *Int. J. Numer. Anal. Meth. Geomech.* **19**, 793–811 (1995).
12. J. P. Carter, M. F. Randolph and C. P. Wroth, 'Stress and pore pressure changes in clay during and after the expansion of a cylindrical cavity', *Int. J. Numer. Anal. Meth. Geomech.*, **3**, 305–323 (1979).
13. M. F. Randolph, J. P. Carter and C. P. Wroth, 'Driven piles in clay — the effects of installation and subsequent consolidation', *Geotechnique*, **29**, 361–393 (1979).
14. I. F. Collins, M. J. Pender and Yang Wang, 'Cavity expansion in sands under drained loading conditions', *Int. J. Numer. Anal. Methods Geomech.* **16**, 3–23 (1992).
15. I. F. Collins, M. J. Pender and Yang Wang, 'Critical state models and the interpretation of penetrometer tests', in: Siriwardane and Zaman (eds), *Computer Methods and Advances in Geomechanics*, Balkema, Rotterdam, Vol. 2, 1994, pp. 1725–1730.
16. K. Been and M. G. Jefferies, 'A state parameter for sands', *Geotechnique*, **35**, 99–112 (1985).
17. I. F. Collins and J. R. Stimpson, 'Similarity solutions for drained and undrained cavity expansions of soils', *Geotechnique*, **44**, 21–34 (1994).
18. R. O. Davis, R. F. Scott and G. Mullenger, 'Rapid expansion of a cylindrical cavity in a rate type soil', *Int. J. Numer. Anal. Methods Geomech.*, **8**, 3–23 (1984).
19. H. S. Yu, 'State parameter from self-boring pressuremeter tests in sand', *J. Geotech. Eng., ASCE*, **120**, 2118–2135 (1995).
20. H. S. Yu, 'Interpretation of pressuremeter unloading tests in sands', *Geotechnique*, in press.
21. A. N. Schofield and C. P. Wroth, *Critical State Soil Mechanics*, McGraw-Hill, New York, 1968.
22. J. H. Atkinson and P. L. Bransby, *The Mechanics of Soils*, Mc-Graw-Hill, New York, 1978.
23. D. Muir Wood, *Soil Behaviour and Critical State Soil Mechanics*, Cambridge University Press, Cambridge, 1990.
24. M. Zytynski, M. F. Randolph, R. Nova and C. P. Wroth, 'On modelling the unloading–reloading behaviour of soils', *Int. J. Numer Anal. Methods Geomech.*, **2**, 87–93 (1978).
25. R. C. Kirby and M. I. Esrig, 'Further development of a general effective stress method for prediction of axial capacity for driven piles in clay', *Recent Development in the Design and Construction of Piles*, ICE, London, pp. 335–344, 1979.
26. M. R. Coop and C. P. Wroth, 'Field studies of an instrumented model pile in clay', *Geotechnique*, **39**, 679–696 (1989).
27. A. J. Bond and R. J. Jardine, 'Effect of installing displacement piles in a high OCR clay', *Geotechnique*, **41**, 341–363 (1991).
28. C. P. Wroth, J. P. Carter and M. F. Randolph, 'Stress changes around a pile driven into cohesive soil', *Recent Development in the Design and Construction of Piles*, ICE, London, Oxford, pp. 345–354, 1979.
29. R. Hill, *The Mathematical Theory of Plasticity*, Oxford University Press, Oxford, 1950.